Estuaries and Coasts (2015) 38 (Suppl 1):S173–S186
DOI 10.1007/s12237-013-9718-9

A Modeling Study of the Potential Water Quality Impacts from In-Stream Tidal Energy Extraction

Taiping Wang · Zhaoqing Yang · Andrea Copping

Received: 26 July 2012 / Revised: 22 August 2013 / Accepted: 26 September 2013 / Published online: 9 November 2013

Abstract To assess the effects of tidal energy extraction on water quality in a simplified estuarine system, which consists of a tidal bay connected to the coastal ocean through a narrow channel where energy is extracted using in-stream tidal turbines, a three-dimensional coastal ocean model with built-in tidal turbine and water quality modules was applied. The effects of tidal energy extraction on water quality were examined for two energy extraction scenarios as compared with the baseline condition. It was found, in general, that the environmental impacts associated with energy extraction depend highly on the amount of power extracted from the system. Model results indicate that, as a result of energy extraction from the channel, the competition between decreased flushing rates in the bay and increased vertical mixing in the channel directly affects water quality responses in the bay. The decreased flushing rates tend to cause a stronger but negative impact on water quality. On the other hand, the increased vertical mixing could lead to higher bottom dissolved oxygen at times. As the first modeling effort directly aimed at examining the impacts of tidal energy extraction on estuarine water quality, this study demonstrates that numerical models can serve as a very useful tool for this purpose. However, more careful efforts are warranted to address system-specific environmental issues in real-world, complex estuarine systems.

Keywords Tidal energy · Numerical model · Water quality · Flushing rate · Vertical mixing

Communicated by Wayne S. Gardner

T. Wang (✉) · Z. Yang · A. Copping
Pacific Northwest National Laboratory, 1100 Dexter Avenue North, Suite 400, Seattle, WA 98109, USA
e-mail: taiping.wang@pnnl.gov

Introduction

In recent years, there has been growing interest in harnessing in-stream tidal energy in response to concerns over increasing energy demand and the associated climate change impacts. Unlike traditional energy sources such as fossil fuels, tidal energy is clean and renewable and has been regarded as a strong candidate for alternative energy in the near future. Research efforts are underway to assess and map tidal energy resources in coastal regions and countries worldwide (e.g., Sutherland et al. 2007; Karsten et al. 2008; Grabbe et al. 2009; O'Rourke et al. 2010; Wang et al. 2011).

Traditionally, tidal energy is extracted using the tidal barrage approach, which mimics conventional hydropower technology by blocking the entrance of a tidal basin with a barrier containing sluices and turbines (Gorlov 2001). Although the tidal barrage approach has been successfully applied in several field sites and could be extended to more places, it raises many environmental concerns due to its significant alternation of the tidal regime (Parker 1993), as well as blocking fish passage and removing virtually all estuarine ecosystem services. Thus, harnessing tidal energy from strong tidal current regions using in-stream (hydrokinetic) tidal devices has quickly gained more attention. A number of studies have been conducted using either analytical or numerical models to evaluate the maximum amount of tidal energy that can be extracted from a tidal system (Garrett and Cummins 2005, 2008; Bryden and Couch 2007; Sutherland et al. 2007; Blanchfield et al. 2008; Draper et al. 2009; Walkington and Burrows 2009; Atwater and Lawrence 2010; Yang et al. 2013). However, these physically based calculations did not consider associated environmental effects, and the calculated energy removal potential is unlikely to be achieved in real-world estuaries and tidal basins. It is, therefore, necessary to assess the potential environmental effects associated with hydrokinetic tidal energy extraction as part of tidal energy resource characterization.

There are a few numerical modeling studies designed to assess the potential effects of tidal energy extraction on hydrodynamics and circulations. For example, by using a three-dimensional (3-D) ocean circulation model, Shapiro (2010) examined the changes in current magnitude and effects on passive tracer transport due to energy extraction. Defne et al. (2011) studied the effects of tidal energy extraction on the estuarine hydrodynamics along the US Georgia coast using the regional ocean modeling system (ROMS). Hasegawa et al. (2011) evaluated the far-field effects of tidal energy extraction in the Minas Passage on tidal circulation in the Bay of Fundy (eastern Canada) and Gulf of Maine (Northeastern USA) using a 3-D nested-grid tidal circulation model based on the Princeton Ocean Model. These studies suggest that the far-field effects of energy extraction on tidal amplitudes and velocities can be substantial, depending on the amounts and locations of tidal energy extracted from the system.

On the other hand, most previous studies on the environmental effects of tidal energy extraction focused only on tidal dynamics (i.e., tidal amplitude and velocity) while neglecting the impacts on other important processes such as estuarine circulation and water quality. In fact, many candidate sites for tidal stream energy extraction are estuarine and coastal waters that are very sensitive to changes in water quality parameters such as dissolved oxygen (DO) (Kadiri et al. 2012). The extraction of tidal energy not only modulates tidal dynamics but also affects water quality through changing the circulation; the degradation of water quality may have ecological consequences in estuaries and coastal waters already stressed by other anthropogenic impacts and climate change. Yang et al. (2013) demonstrated that tidal energy extraction could have a large impact on the flushing rates in a tidal basin. Yang and Wang (2013a) further examined the impacts of tidal energy extraction on baroclinic circulation and mixing in the tidal system. In this study, we extended our modeling effort to directly assess the potential effects on water quality resulting from tidal energy extraction using a similar tidal channel and bay system.

Methods

Model Description

The model used in this study is the widely used finite-volume coastal ocean model (FVCOM) developed by Chen et al. (2003, 2006). As a prognostic, unstructured-grid, finite-volume, 3-D primitive equation coastal ocean circulation model, FVCOM has been extensively used by the estuarine and coastal modeling community to solve a variety of scientific problems related to both physical and biological processes (e.g., Weisberg and Zheng 2006; Ji et al. 2008; Chen et al. 2009, 2012; Hu et al. 2011; Yang et al. 2012; Yang and Wang 2013b). FVCOM simulates water surface elevation, velocity, salinity, temperature, sediment, and other scalar constituents in an integral form by computing fluxes between nonoverlapping horizontal triangular control volumes. This unstructured-grid and finite-volume approach combines the advantages of finite-element methods for geometric flexibility and finite-difference methods for simple discrete structures and computational efficiency (Chen et al. 2007). In addition, it provides a reliable numerical representation of both local and global momentum and mass conservation. In the vertical direction, a sigma-stretched coordinate is used to better represent the irregular bottom topography in the coastal regions. The detailed theoretical aspects and model formulations of FVCOM have been presented in Chen et al. (2003, 2006, 2007) and other FVCOM publications and thereby will not be elaborated here.

In our previous work, a tidal turbine module was developed for FVCOM based on the widely used momentum sink approach (Yang et al. 2013). Specifically, the momentum sink induced by turbines can be defined as follows:

$$\overrightarrow{F^{\mathrm{M}}} = \frac{1}{2}\frac{C_{\mathrm{e}}A}{V_{\mathrm{c}}}\left|\vec{u}\right|\vec{u} \tag{1}$$

where $\overrightarrow{F^{\mathrm{M}}}$ is the momentum sink rate from a momentum control volume V_{c} by tidal turbines (in meters per second squared), C_{e} is the momentum extraction coefficient, A is the flow-facing area of the turbines or the turbine swept area (in square meters), and $\vec{u}$ is the velocity vector (in meters per second). The quadratic form of Eq. 1 is similar to the momentum sink terms used by others (Defne et al. 2011; Hasegawa et al. 2011) and the detailed formulations and validation experiments can be seen in the study of Yang et al. (2013).

Water Quality Model Development

To simulate water quality responses resulting from tidal energy extraction, a nitrogen-based water quality model was incorporated into FVCOM. The general structure and formulations of the model were based mainly on the biological model in ROMS (Fennel et al. 2006; Gruber et al. 2006; Bianucci et al. 2011) and were modified by referencing to other well-established estuarine eutrophication models including CE-QUAL-ICM (Cerco and Cole 1993, 1994; Cerco and Noel 2004) and three-dimensional hydrodynamic-eutrophication model (HEM-3D) (Park et al. 1995, 2005). The mass conservation and transport equation for any water quality variable is given by

$$\frac{\partial C}{\partial t}+\frac{\partial (uC)}{\partial x}+\frac{\partial (vC)}{\partial y}+\frac{\partial (wC)}{\partial z}=\frac{\partial}{\partial x}\left(K_x\frac{\partial C}{\partial x}\right)+\frac{\partial}{\partial y}\left(K_y\frac{\partial C}{\partial y}\right)+\frac{\partial}{\partial z}\left(K_z\frac{\partial C}{\partial z}\right)+R+W \tag{2}$$

where C is the concentration of the water quality variable at each node; u, v, and w are the velocity components in the x, y,

and z directions, respectively; K_x, K_y, and K_z are the eddy diffusivities in the x, y, and z directions, respectively; R represents the source and sink processes of water quality variables through kinetic reactions, settling, air–sea exchange, and benthic flux; and W is the external loading directly added to each node. In the current model configuration, all external loadings are assumed to enter the model domain at river boundaries. Hence, the external loading term W is not implemented in the current model.

In this study, seven coupled state variables are considered: phytoplankton (Phy), zooplankton (Zoo), nitrate (NO_3), ammonium (NH_4), detritus nitrogen (DetN), detritus carbon (DetC), and dissolved oxygen (DO). These variables form the most fundamental biological processes in nitrogen-limited marine ecosystems; the concentrations are based on nitrogen units (in grams N per cubic meter), except for DetC and DO, which have units of grams C per cubic meter and grams O_2 per cubic meter, respectively. In another words, the state variables (except for DO and DetC) represent concentrations of nitrogen within different state variable pools. The source and sink processes of the water quality model are illustrated in Fig. 1. The source terms for phytoplankton (which plays a central role in the water quality model) include growth (photosynthesis supported by N uptake) and sink terms include basal metabolism, grazing by zooplankton, mortality, and settling. It is assumed that zooplankton assimilates ingested phytoplankton with the efficiency β, while the remaining fraction is transferred to the detrital nitrogen pool. Other zooplankton sink terms include basal metabolism, egestion through fecal pellets, and mortality. The source term for nitrate is nitrification from ammonium; the sink term is uptake by phytoplankton. For ammonium, the source terms include excretion by phytoplankton and zooplankton through basal metabolism and remineralization of DetN; the sink terms are phytoplankton uptake and nitrification. For ammonium in the bottom layer, there is an additional source contributed by benthic flux from the sediment. The source terms for DetN and DetC come mainly from the sink terms of phytoplankton and zooplankton. The sink terms are remineralization into ammonium and CO_2, respectively. For DO, one of the most important water quality variables, photosynthesis, is the primary source term, while sink terms include nitrification, consumption by phytoplankton and zooplankton through basal metabolism, and remineralization of DetC. In addition, DO in the surface layer is affected by the air–sea exchange or surface re-aeration process, which can be either the source or sink term depending on the saturation level of surface DO. DO in the bottom layer is also affected by sediment oxygen demand (SOD) released from bottom sediment. Phytoplankton and detritus can also be lost in the model by settling out as particles to the seafloor. For each state variable, the full set of source and sink terms R in Eq. 2 are written as:

$$\frac{\partial[\mathrm{Phy}]}{\partial t} = \mu_{\mathrm{p}}^{\max}\cdot f(I)\cdot f(T)\cdot f(N)\cdot[\mathrm{Phy}] - p_{\mathrm{bmet}}\cdot[\mathrm{Phy}] - p_{\mathrm{mort}}\cdot[\mathrm{Phy}] - z_{\mathrm{graze}}\cdot[\mathrm{Zoo}]\cdot\frac{[\mathrm{Phy}]}{K_{\mathrm{p}}+[\mathrm{Phy}]} - L_{\mathrm{vs}} \tag{3}$$

$$\frac{\partial[\mathrm{Zoo}]}{\partial t} = z_{\mathrm{graze}}\cdot\beta\cdot[\mathrm{Zoo}]\cdot\frac{[\mathrm{Phy}]}{K_{\mathrm{p}}+[\mathrm{Phy}]} - z_{\mathrm{bmet}}\cdot[\mathrm{Zoo}] - z_{\mathrm{eg}}\cdot[\mathrm{Zoo}] - z_{\mathrm{mort}}\cdot[\mathrm{Zoo}]^2 \tag{4}$$

$$\frac{\partial[\mathrm{NO_3}]}{\partial t} = -\mu_{\mathrm{p}}^{\max}\cdot f(I)\cdot f(T)\cdot f(N)\cdot Q_{\mathrm{NP}}\cdot[\mathrm{Phy}] + Q_{\mathrm{nitr}}\cdot[\mathrm{NH_4}] \tag{5}$$

$$\frac{\partial[\mathrm{NH_4}]}{\partial t} = -\mu_{\mathrm{p}}^{\max}\cdot f(I)\cdot f(T)\cdot f(N)\cdot Q_{\mathrm{RP}}\cdot[\mathrm{Phy}] - Q_{\mathrm{nitr}}\cdot[\mathrm{NH_4}] + p_{\mathrm{bmet}}\cdot[\mathrm{Phy}] + z_{\mathrm{bmet}}\cdot[\mathrm{Zoo}] + d_{\mathrm{remin}}\cdot[\mathrm{DetN}] + \frac{J_{\mathrm{NH_4}}}{\Delta Z_{\mathrm{b}}} \tag{6}$$

$$\frac{\partial[\mathrm{DetN}]}{\partial t} = z_{\mathrm{graze}}\cdot(1-\beta)\cdot[\mathrm{Zoo}]\cdot\frac{[\mathrm{Phy}]}{K_{\mathrm{p}}+[\mathrm{Phy}]} + p_{\mathrm{mort}}\cdot[\mathrm{Phy}] + z_{\mathrm{eg}}\cdot[\mathrm{Zoo}] + z_{\mathrm{mort}}\cdot[\mathrm{Zoo}]^2 - d_{\mathrm{remin}}\cdot[\mathrm{DetN}] - L_{\mathrm{vs}} \tag{7}$$

$$\frac{\partial[\mathrm{DetC}]}{\partial t} = \left(z_{\mathrm{graze}}\cdot(1-\beta)\cdot[\mathrm{Zoo}]\cdot\frac{[\mathrm{Phy}]}{K_{\mathrm{p}}+[\mathrm{Phy}]} + p_{\mathrm{mort}}\cdot[\mathrm{Phy}]\right)\cdot r_{\mathrm{C/N,phy}} + z_{\mathrm{eg}}\cdot[\mathrm{Zoo}]\cdot r_{\mathrm{C/N,zoo}} + z_{\mathrm{mort}}\cdot[\mathrm{Zoo}]^2\cdot r_{\mathrm{C/N,zoo}} - d_{\mathrm{remin}}\cdot[\mathrm{DetC}] - L_{\mathrm{vs}} \tag{8}$$

$$\frac{\partial[\mathrm{DO}]}{\partial t} = \mu_{\mathrm{p}}^{\max}\cdot f(I)\cdot f(T)\cdot f(N)\cdot\left(Q_{\mathrm{NP}}\cdot r_{\mathrm{O_2/NO_3}} + Q_{\mathrm{RP}}\cdot r_{\mathrm{O_2/NH_4}}\right)\cdot[\mathrm{Phy}] - Q_{\mathrm{nitr}}\cdot[\mathrm{NH_4}]\cdot r_{\mathrm{nitr,O_2/NH_4}} - p_{\mathrm{bmet}}\cdot r_{\mathrm{O_2/NH_4}}\cdot[\mathrm{Phy}] - z_{\mathrm{bmet}}\cdot r_{\mathrm{O_2/NH_4}}\cdot[\mathrm{Zoo}] - d_{\mathrm{remin}}\cdot[\mathrm{DetC}]\cdot r_{\mathrm{O_2/C}} + k_{\mathrm{r}}\cdot(\mathrm{DO_s}-[\mathrm{DO}]) - \frac{\mathrm{SOD}}{\Delta Z_{\mathrm{b}}} \tag{9}$$

In Eqs. 3, 7, and 8, the term L_{vs} on the right-hand side denotes loss via settling, which has the following general form:

$$L_{\mathrm{vs}} = w_{\mathrm{s}}\frac{\partial[C]}{\partial z} \tag{10}$$

where w_{s} is the settling velocity and C denotes the water quality variables subject to vertical settling and correspond to Phy, DetN, and DetC in Eqs. 3, 7, and 8, respectively. In Eq. 3, $\mu_{\mathrm{p}}^{\max}$ is the phytoplankton maximum growth rate under the optimal environmental conditions; $f(I)$, $f(T)$, and $f(N)$ are the limiting functions for light, temperature, and nitrogen, respectively. For the light limiting function, the classic Michaelis–Menten type relationship was used here:

$$f(I) = \frac{I}{k_I + I} \tag{11}$$

where I is the light intensity for photosynthetically active radiation (PAR), which roughly equals to 43 % of total solar

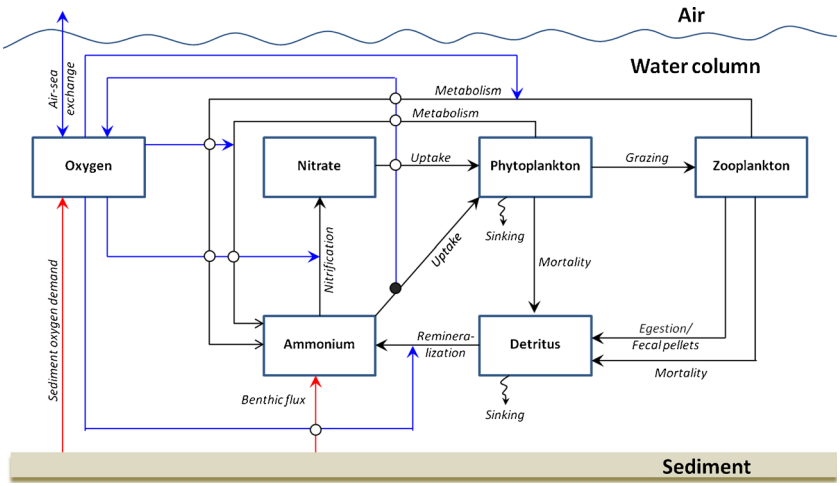

Fig. 1 Flow diagram depicting kinetic interactions of the water quality model. *Boxes* represent model state variables and the *arrows* show the processes that transfer mass between different state variables. *Open circles intersected by arrows* denote there are no interactions, while *solid circles* denote interactions among them

radiation at the sea surface, and k_I is the half-saturation light intensity. The commonly used Lambert–Beer law for light extinction was used to define the extinction of light with water depth:

$$\frac{\mathrm{d}I(z)}{\mathrm{d}z} = -(k_\mathrm{w} + k_\mathrm{chla}\cdot\mathrm{chla}(z))\cdot I(z) \tag{12}$$

where k_w is the background light extinction coefficient of seawater, k_chla is the light extinction coefficient due to phytoplankton self-shading, and chla(z) is the phytoplankton concentration represented as chlorophyll a. The relationship between chlorophyll a and phytoplankton is defined as:

$$\mathrm{chla}(z) = \theta\cdot[\mathrm{phy}(z)] \tag{13}$$

where θ is the fixed ratio of chlorophyll a to nitrogen for phytoplankton. For the temperature effect on phytoplankton growth, the Gaussian probability curve type formula used in HEM-3D was adopted (Park et al. 1995):

$$\begin{aligned} f(T) &= \exp^{\left(-\mathrm{KTG1}\left[T-T_\mathrm{opt}\right]^2\right)} \quad \text{when } T \le T_\mathrm{opt} \\ &= \exp^{\left(-\mathrm{KTG2}\left[T_\mathrm{opt}-T\right]^2\right)} \quad \text{when } T > T_\mathrm{opt} \end{aligned} \tag{14}$$

where T is the water temperature, T_opt is the optimal temperature for phytoplankton growth, and KTG1 and KTG2 are the coefficients. p_bmet, p_mort, and z_graze are the rates for phytoplankton basal metabolism, mortality, and zooplankton grazing, respectively. k_p is the half-saturation constant. The nitrogen limiting function $f(N)$ is defined as:

$$f(N) = Q_\mathrm{NP} + Q_\mathrm{RP} \tag{15}$$

where Q_NP and Q_RP are the N limiting functions by nitrate and ammonium, respectively. Considering the preference for ammonium uptake, they are further defined as:

$$Q_\mathrm{NP} = \frac{[\mathrm{NO_3}]}{K_{\mathrm{NO_3}} + [\mathrm{NO_3}]}\cdot\frac{K_{\mathrm{NH_4}}}{K_{\mathrm{NH_4}} + [\mathrm{NH_4}]} \tag{16}$$

$$Q_\mathrm{RP} = \frac{[\mathrm{NH_4}]}{K_{\mathrm{NH_4}} + [\mathrm{NH_4}]} \tag{17}$$

where $K_{\mathrm{NO_3}}$ and $K_{\mathrm{NH_4}}$ are the half-saturation constants for nitrate and ammonium uptake by phytoplankton, respectively.

In Eq. 4, β stands for zooplankton grazing efficiency, z_bmet, z_eg, and z_mort are rates for zooplankton basal metabolism, egestion through fecal pellets, and mortality, respectively. In Eq. 5, the nitrification rate is defined as:

$$Q_\mathrm{nitr} = t_\mathrm{nitr}\cdot\left(1-\max\left[0,\frac{\mathrm{PAR}(z)-I_{\mathrm{thNH_4}}}{D_{\mathrm{p5NH_4}} + \mathrm{PAR}(z)-I_{\mathrm{thNH_4}}}\right]\right) \tag{18}$$

where t_nitr is the maximum nitrification rate, $I_{\mathrm{thNH_4}}$ is the threshold PAR for nitrification inhibition, and $D_{\mathrm{p5NH_4}}$ is the half-saturation light intensity for nitrification inhibition. In Eqs. 6, 7, and 8, d_remin stands for the remineralization rate of detritus. In Eq. 6, $J_{\mathrm{NH_4}}$ denotes the benthic ammonium flux rate for the bottom layer of the water column and ΔZ_b is the bottom layer thickness. In Eq. 8, $r_{\mathrm{C/N,phyto}}$ and $r_{\mathrm{C/N,zoo}}$ are the cellular carbon-to-nitrogen ratios for phytoplankton and zooplankton, respectively. In Eq. 9, $r_{\mathrm{O_2/NO_3}}$ and $r_{\mathrm{O_2/NH_4}}$ are the stoichiometry ratios for oxygen production during photosynthesis using nitrate and ammonium as N source, respectively; $r_{\mathrm{nitr,O_2/NH_4}}$ is the oxygen-to-ammonium ratio for nitrification and $r_{\mathrm{O_2/C}}$ is the oxygen-to-carbon ratio for DetC.

For deep estuaries like fjords, the DO surface re-aeration rate k_r in Eq. 9 mainly depends on the effect of turbulence generated by surface wind stress (Cerco and Noel 2004). For simplification, it was assumed to be constant in this study. The saturated DO concentration ($\mathrm{DO_s}$) is

determined using the same equation as that used in HEM-3D (Park et al. 1995) and has the following form:

$$DO_s = 14.5532 - 0.38217 \cdot T + 5.4258 \times 10^{-3} \cdot T^2 - \frac{S}{1.80655} \cdot \left(1.665 \times 10^{-4} - 5.866 \times 10^{-6} \cdot T + 9.796 \times 10^{-8} \cdot T^2\right) \quad (19)$$

where T and S stand for water temperature and salinity, respectively. The last term on the right-hand side of Eq. 9 represents the effect of SOD.

To calculate the benthic flux of ammonium J_{NH_4} and SOD, we adopted the sediment component model developed by Bianucci et al. (2011). This model is a much improved version of the original sediment component model by Fennel et al. (2006) for the biological model in ROMS. The detailed model formulations and parameter configurations were provided by Bianucci et al. (2011) and, thus, will not be described here. The water quality state variables are solved using the same transport scheme as salinity and temperature. The kinetic equations are updated explicitly at each internal time step. Table 1 lists all the parameters, values, and units used for this study. The parameter values are mostly adopted from literature without further adjustment. However, the parameter values should be further calibrated based on field data for model applications in real estuarine environments.

Study Domain

To examine the impacts of tidal energy extraction on water quality in a more general setting, we started with an idealized model domain with simplified geometry. The study domain is similar to the tidal channel–bay system of Yang et al. (2013) and was designed with dimensions similar to those of Puget Sound, a representative fjord-like estuary with a large tidal range in the Pacific Northwest, USA. Puget Sound is considered a promising candidate for tidal energy extraction. The study domain consists of a large tidal bay that is forced by both river discharge upstream and by tides entering through a narrow channel connecting to a much broader coastal ocean (Fig. 2). The tidal bay and channel system roughly mimics Puget Sound and its Admiralty Inlet entrance. Table 2 shows the dimensions of the model domain. The entire domain is covered by an unstructured grid consisting of 25,415 triangular elements and 13,148 nodes. The model element size varies from 300 m in the tidal channel to nearly 4,500 m at the coastal ocean boundary. In the vertical direction, 10 sigma layers are specified.

Model Forcing

Simulating water quality in the coastal environment requires extensive forcing information on nutrient loadings, freshwater discharge, meteorological forcing, and ocean boundary conditions. In this study, all the forcing functions were constructed from observational data in the Puget Sound region. For tidal forcing, two tidal constituents, the principal lunar semidiurnal tide (M_2) and the principal solar semidiurnal tide (S_2), with amplitudes of 0.7 and 0.3 m, respectively, were specified at the ocean boundary to represent the spring–neap tidal cycle. For the upstream river boundary, daily flows and temperatures were generated based on the climatology river inflows of Puget Sound. As can be seen in Fig. 3a, the hydrograph shows a distinct seasonal pattern with peak flows occurring in late fall and winter, primarily driven by high precipitation.

Long-term river temperature records in Puget Sound are limited. Existing temperature measurements for major rivers emptying into Puget Sound showed relatively small seasonal variations. An idealized river annual temperature distribution was, thus, developed based on 3 years of temperature records in the Cedar River that discharges into the main basin of Puget Sound. The annual temperature follows a sinusoidal curve with a maximum temperature of 16 °C in July and a minimum temperature of 6 °C in January (Fig. 3b). Similarly, two sinusoidal curves were constructed, respectively, for daily maximum and minimum temperature values based on the measurements at the National Oceanic and Atmospheric Administration (NOAA) weather station in Seattle, Washington. The idealized hourly temperature–time series were then generated based on the sinusoidal daily maximum and minimum temperature curves. The comparisons between constructed air temperature–time series and NOAA observations are shown in Fig. 3c, d.

Solar radiation and net heat flux at the air–water interface are required in FVCOM for water temperature simulation using the prescribed heat flux scheme. Due to limited observational data in Puget Sound, a combination approach was used to generate the required meteorological forcing utilizing NOAA observations, model predictions by the Weather Research and Forecast Model, and empirical formulas. The solar radiation shown in Fig. 3e, f is calculated based on the formula of the CE-QUAL-W2 model (Cole and Wells 2009). The detailed steps for net heat flux calculations were described by Yang et al. (2011). In Fig. 3g, h, the negative net heat flux values represent heat release from water to the atmosphere, normally occurring at night. Tidal boundary conditions were specified every 15 min, while river and meteorological inputs were specified at hourly intervals. In the current study, wind forcing was not included due to the highly stochastic distributions in both time and space.

All nutrient loadings were assumed to enter the model domain through river discharges. To simplify the problem, nutrient concentrations (i.e., nitrate, ammonium, and DetN) were specified as constant values in time based on observational data for major rivers emptying into Puget Sound.

Table 1 Definitions, values, and units for the parameters of the water quality model

Parameter	Symbol	Value	Unit
Phytoplankton parameters			
Phytoplankton maximum growth rate	μ_p^{max}	2.5[a]	day^{-1}
Light attenuation coefficient due to seawater	k_w	0.2[b]	m^{-1}
Light attenuation coefficient due to chlorophyll *a*	k_{chla}	0.024[c]	m^2(mg Chla)$^{-1}$
Half-saturation light intensity for phytoplankton growth	k_I	30.0[b]	W m^{-2}
Optimum temperature for phytoplankton growth	T_{opt}	15.0[b]	°C
Coefficient for effect of temperature below T_{opt} on growth	KTG1	0.004[a]	$°C^{-2}$
Coefficient for effect of temperature above T_{opt} on growth	KTG2	0.006[a]	$°C^{-2}$
Cellular C/N ratio for phytoplankton	$r_{C/N,phyto}$	5.68[b]	g C(g N)$^{-1}$
Cellular chlorophyll *a*/N ratio	θ	0.114[a]	g Chla(g N)$^{-1}$
Half-saturation N concentration for nitrate uptake	k_{NO_3}	0.01[d]	g N m^{-3}
Half-saturation N concentration for ammonium uptake	k_{NH_4}	0.007[d]	g N m^{-3}
Phytoplankton basal metabolism rate	p_{bmet}	0.01[a]	day^{-1}
Phytoplankton linear mortality rate	p_{mort}	0.072[d,e]	day^{-1}
Zooplankton parameters			
C/N ratio for zooplankton	$r_{C/N,zoo}$	5.68[b]	g C(g N)$^{-1}$
Zooplankton grazing rate	z_{graze}	0.6[d]	day^{-1}
Zooplankton assimilation efficiency	β	0.75[d,e]	–
Zooplankton half-saturation constant for ingestion	K_p	0.014[d]	g N m^{-3}
Zooplankton egestion rate	z_{eg}	0.1[c]	day^{-1}
Zooplankton quadratic mortality to detritus	z_{mort}	7.0[d,e]	day^{-1}(g N m^{-3})$^{-1}$
Zooplankton basal metabolism rate	z_{bmet}	0.1[c]	day^{-1}
Remineralization parameters			
Detritus remineralization rate	d_{remin}	0.02[d]	day^{-1}
Nitrification rate in the dark	t_{nitr}	0.05[d]	day^{-1}
Threshold PAR for nitrification inhibition	I_{thNH_4}	0.01[d]	W m^{-2}
Half-saturation PAR for nitrification inhibition	D_{p5NH_4}	0.036[d]	W m^{-2}
DO parameters			
Oxygen/nitrate stoichiometry for photosynthesis	r_{O_2/NO_3}	19.71[b]	g O_2(g N)$^{-1}$
Oxygen/ammonium stoichiometry for photosynthesis	r_{O_2/NH_4}	15.14[a]	g O_2(g N)$^{-1}$
Oxygen/ammonium stoichiometry for nitrification	$r_{nitr,O_2/NH_4}$	2.28[a]	g O_2(g N)$^{-1}$
Oxygen/carbon stoichiometry	$r_{O_2/C}$	2.67[a]	g O_2(g C)$^{-1}$
Surface re-aeration rate for DO	k_r	1.0[b]	m day^{-1}
Sinking parameters			
Sinking velocity for detritus	w_D	2.0[d]	m day^{-1}
Sinking velocity for phytoplankton	w_{Phy}	0.2[a,d,e]	m day^{-1}

[a] Park et al. (2005)
[b] Bowie et al. (1985)
[c] Bianucci et al. (2011)
[d] Gruber et al. (2006)
[e] Fennel et al. (2006)

Therefore, the loading rates are basically a function of the river discharge rate, which varies throughout the year. Similarly, concentrations of phytoplankton, zooplankton, and DetC were also simplified as constants at the river boundary. For DO, considering its significant seasonal variations due to river temperature, the concentrations at the river boundary were calculated as a function of river temperature using Eq. 19.

At the ocean boundary, salinity, temperature, and all water quality state variables were specified as constants in the current study; this simplified treatment is sufficient because the ocean boundary is far enough from the tidal bay (170 km away from the entrance of the tidal channel) and the variations of salinity, temperature, and water quality constituents at the ocean boundary are much smaller than those inside the bay. The concentrations at both the ocean and river boundaries are provided in Table 3.

Design of Numerical Model Experiments

To evaluate the impacts of tidal energy extraction on water quality, a baseline condition without any tidal energy extraction was first established (experiment 1). Two energy extraction scenarios were then conducted to assess the corresponding

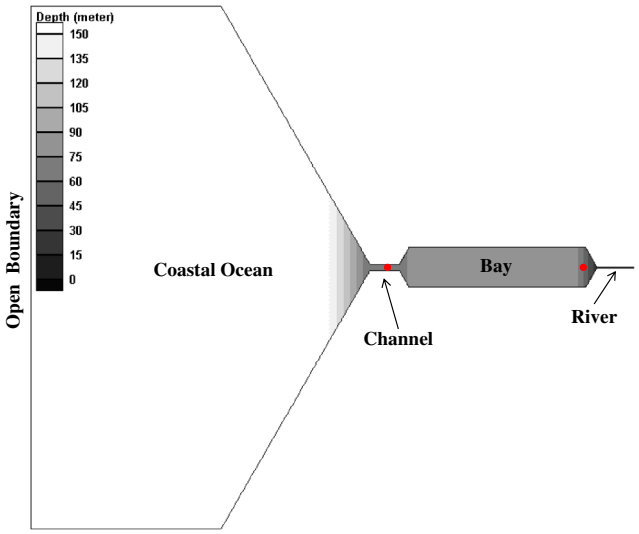

Fig. 2 The model domain with simplified geometry. The *two dots* located in the middle of the tidal channel and upper bay denote the locations where velocity and water quality time series data were analyzed

water quality impacts based on both the turbine efficiency curve (Fig. 4) and the power potential curve (Yang and Wang 2013a). In the first energy extraction scenario (experiment 2), 300 MW tidally averaged power (about 40 % of the maximum extractable power) was extracted from the system with 1,500 turbines deployed in the tidal channel. Under this scenario, the turbine efficiency remains relatively high (Fig. 4). In the second energy extraction scenario (experiment 3), the number of tidal turbines was increased to 15,000 turbines. The extracted power increases to 760 MW, which approximately corresponds to the maximum extractable power but at a much lower turbine efficiency. In both experiments 2 and 3, tidal turbines were evenly distributed in the tidal channel at a depth of 10 m above the seafloor. The momentum extraction coefficient by turbines was specified as 0.5, based on our previous study (Yang et al. 2013).

To reduce the effects of initial conditions on model results, all model simulations were configured to run continuously for 4 years by repeating the constructed model forcing for each year. A sufficiently long "spin-up" time allows the model to reach a stabilized condition necessary for reliable evaluations of the results. The model results also suggest that the model approached dynamic equilibrium after 2 years of continuous simulation. The results in the fourth year were processed and compared to assess the impacts resulting from energy extraction.

Table 2 Dimensions of the model domain

Sub-domain	Length (m)	Width (m)	Depth (m)
Coastal ocean	170,000	250,000	150
Tidal channel	15,000	3,000	60
Semi-enclosed bay	100,000	20,000	80

Results and Discussion

Hydrodynamic Response of the System to Tidal Energy Extraction

The first effect of tidal energy extraction examined in this study is changes in tidal velocity. The extraction of tidal energy from the channel affects tidal velocity, as evidenced by the velocity results at the station located in the middle of the channel (for station location, see Fig. 2). Figure 5 shows the 1-day time series comparisons of depth-averaged velocity for both the baseline condition and the two energy extraction experiments during spring tide. The results demonstrate, in general, that more power extraction leads to a greater reduction in tidal velocity and an increase in tidal phase shift. For the 300-MW experiment, the changes in tidal velocity are relatively small. Because tidal amplitude inside the bay is controlled by tidal flows through the channel, the corresponding changes of tidal amplitude inside the bay are also small, which is confirmed by further examination of the model results inside the bay.

Water Quality Condition for the Baseline Scenario

The station located in the upper bay (Fig. 2) was selected as an example of the baseline water quality distributions in an area heavily affected by nutrient inputs from the river and also sensitive to change in water circulation. Figure 6 shows the water quality time series for surface and bottom layers of the water column. It can be seen that most water quality variables exhibit strong temporal variations at timescales controlled by seasonal cycles of meteorological and river forcing, tides, and the diurnal solar cycle.

Phytoplankton exhibits seasonality, as shown in Fig. 6a, with surface phytoplankton (chlorophyll *a*) reaching a maximum (>30 μg L^{-1}) during the period from late spring to early summer, driven by high nutrient loadings and increased water temperature and solar radiation. Phytoplankton remains light-limited in bottom waters and seldom reaches 5 μg L^{-1} of chlorophyll *a* throughout the year. Surface phytoplankton concentrations also vary substantially throughout the day, affected by both tides and the diurnal solar cycle. For instance, during the growing seasons in late spring, surface chlorophyll *a* can vary by as much as 10 μg L^{-1} in a day. DO is the primary concern for many anthropogenically disturbed ecosystems. The model results suggest that DO concentrations remain sufficiently high (e.g., >5 mg L^{-1}) throughout the year to support biological activities (Fig. 6b). It is noteworthy that bottom water DO was affected by spring–neap tidal cycle, especially during late summer when DO reaches annual minima. The lowest DO tends to occur immediately following the neap tide. It is believed that reduced vertical mixing during the neap tide causes this decrease in bottom DO.

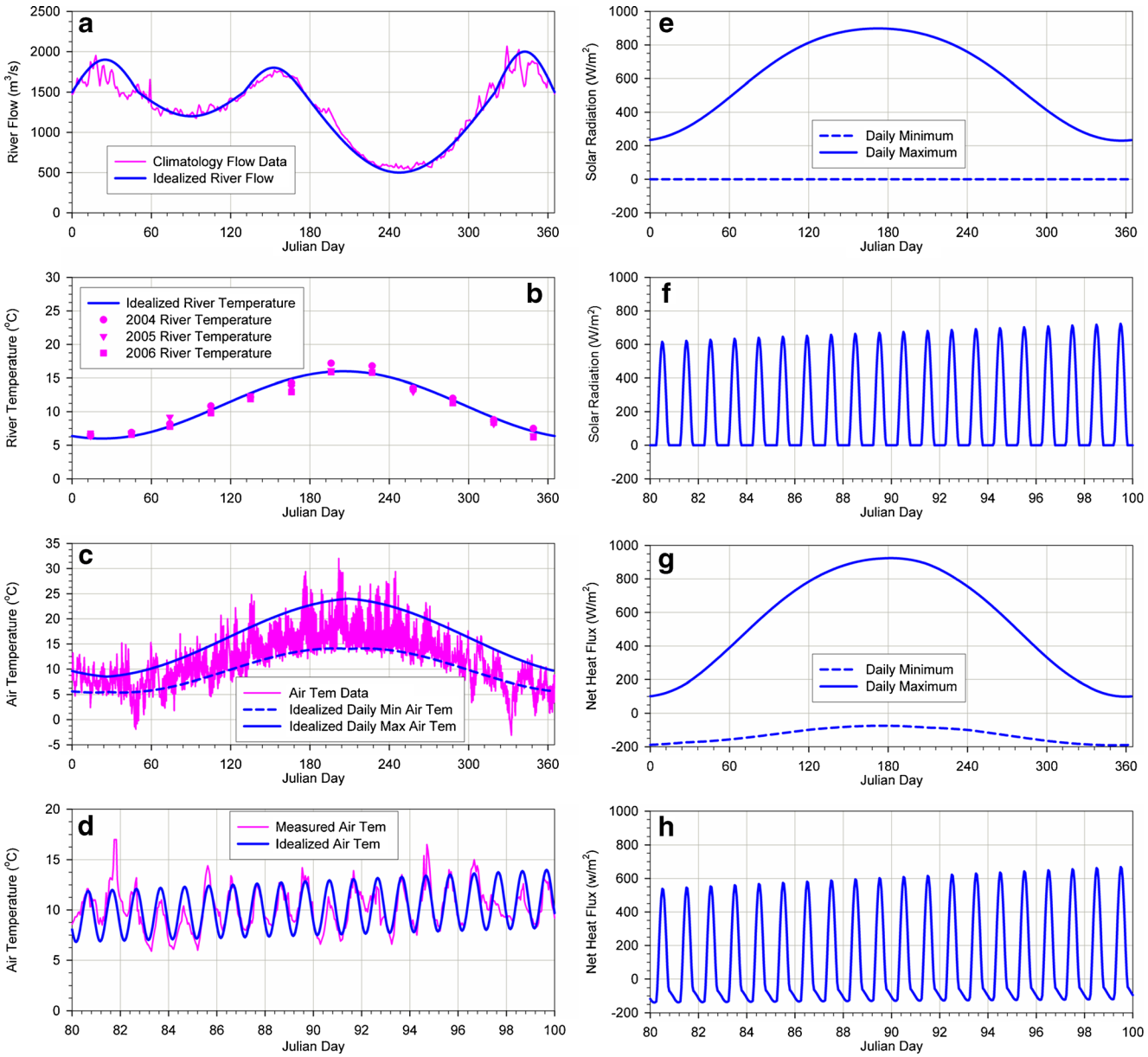

Fig. 3 Constructed model forcing time series from climatology data in Puget Sound for river inflow (**a**), temperature (**b**), air temperature (**c**, **d**), solar radiation (**e**, **f**), and net heat flux (**g**, **h**)

For inorganic N, the model reproduced the appropriate seasonal patterns. For example, ammonium, which relies mainly on in situ recycling/regeneration processes in the sediment and water column, tends to remain relatively stable throughout the year but often increases in summer and fall in bottom waters. The model successfully captures this temporal trend (Fig. 6c). Nitrate has a distinct seasonal pattern that is high in winter–spring (due to high river inputs) and lower in summer (due to rapid uptake by autotrophs). This seasonal pattern is well captured by the model (Fig. 6d). DetN is largely controlled by the balance between in situ production (source) and decomposition (sink) processes and tends to remain relatively constant in coastal waters, as confirmed by the model results (Fig. 6e). DetC is regulated by in situ production and decomposition/settling processes, but unlike DetN, DetC is also heavily affected by river input and exhibits a seasonal pattern that closely follows the variability of river input (Fig. 6f).

The model results have been shown to be capable of reproducing the typical water quality conditions for temperate fjords receiving relatively low nutrients from rivers. The established baseline scenario demonstrates the natural condition with good water quality, prior to the introduction of tidal energy extraction.

Table 3 Boundary and initial conditions of the water quality model

Variable (unit)	Open boundary concentration	River boundary concentration	Initial concentration
Phy (g N m^{-3})	0.05	0.05	0.05
Zoo (g N m^{-3})	0.005	0.01	0.01
NO_3 (g N m^{-3})	0.01	1.0	0.1
NH_4 (g N m^{-3})	0.01	0.01	0.01
DetN (g N m^{-3})	0.05	0.1	0.1
DetC (g C m^{-3})	1.0	4.0	1.0
DO (g $O_2 m^{-3}$)	7.46	Calculated using Eq. 19	8.0

Water Quality Responses to Tidal Energy Extraction

Phytoplankton primary production provides the foundation for marine ecosystems; thus, it is crucial to examine how phytoplankton will respond to tidal energy extraction from the system. Figure 7 shows the surface phytoplankton concentrations at the same upper bay station for both the baseline and tidal energy extraction scenarios. To better illustrate the results, the model results were first processed with a 36-h low-pass filter to remove the high-frequency (e.g., semidiurnal and diurnal) oscillations. Based on the low-pass filtered time series, in general, phytoplankton concentrations do not show substantial changes for either energy extraction experiment, as compared with the baseline condition. For the 760-MW experiment, phytoplankton shows elevated concentrations as compared with the baseline condition. The increases appear to be larger during spring tides. In comparison, for the 300-MW experiment, the changes in chlorophyll *a* concentration are within 1 μg L^{-1}.

Concerns about potential effects of tidal energy extraction on DO relate to the effects that those changes might have on heterotrophic organisms such as fishes. For fjord-like systems such as Puget Sound, deep bottom waters are most likely to suffer from decreased DO levels (e.g., Newton et al. 2007). The annual minimum daily averaged bottom DO concentrations along the longitudinal axis of the tidal bay were examined based on model results for the entire year. The longitudinal distributions of minimum daily averaged bottom DO under all three experimental conditions are presented in Fig. 8. As one can see, DO exhibits somewhat similar longitudinal patterns for all three scenarios with minimum concentrations generally occurring in the middle to upper bay regions. This is also consistent with estuaries such as Chesapeake Bay (Officer et al. 1984) and Hood Canal (Newton et al. 2007). Under the baseline condition, the minimum DO concentrations are generally close to 5 mg L^{-1}, a level that is commonly assumed to be sufficient for aquatic organisms. However, in the 760-MW experiment, minimum DO concentrations show a general decrease from the baseline condition in regions spanning a 50-km distance. The minimum DO concentrations drop substantially to <4 mg L^{-1} in the middle bay. The maximum difference also exceeds 1 mg L^{-1}. Interestingly, no obvious changes of DO concentrations were observed for the 300-MW experiment. It can be seen that, near both ends of the bay, minimum DO concentrations actually

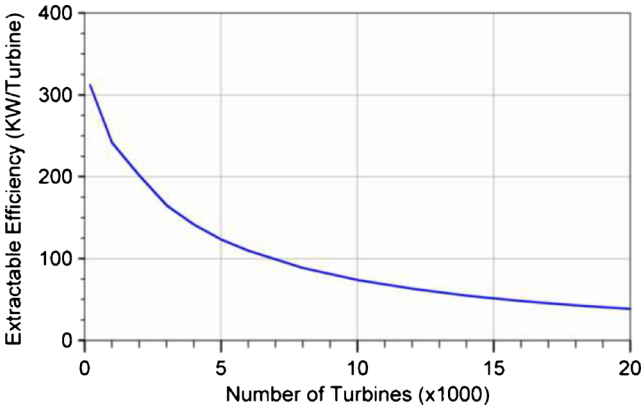

Fig. 4 Turbine efficiency curve. Note that the efficiency decreases as the total number of turbines increases

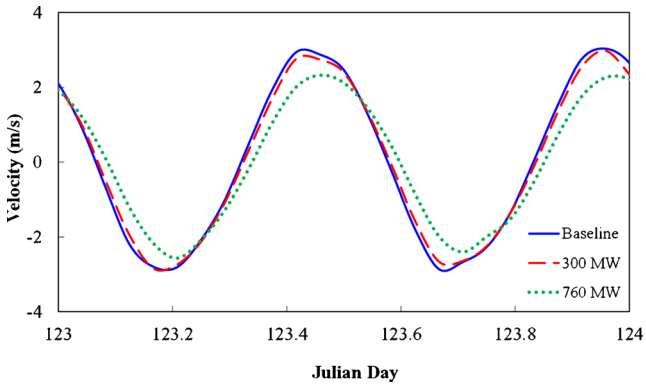

Fig. 5 Tidal velocity responses to tidal energy extraction as compared with the baseline condition. The results were depth-averaged velocities extracted at the channel station during spring tide

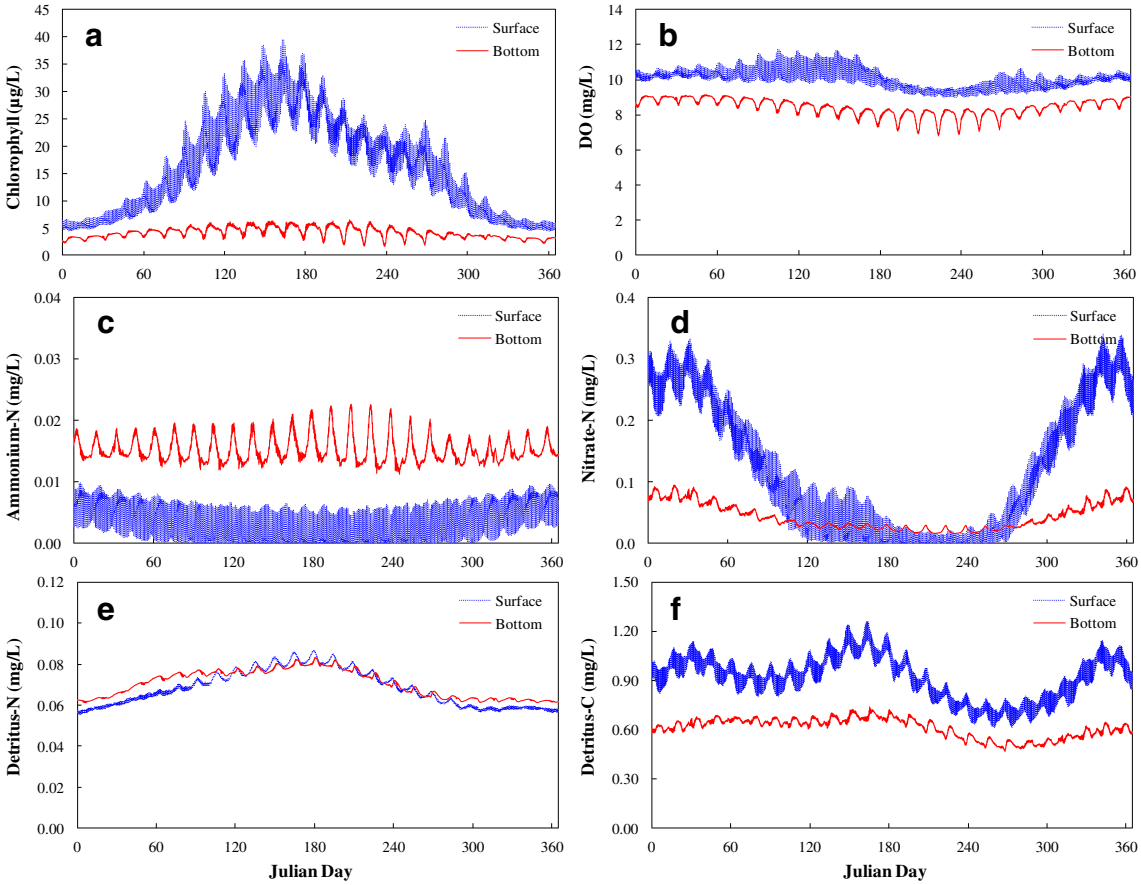

Fig. 6 Time series plots of water quality variables for the baseline condition at the upper bay station: phytoplankton/chlorophyll *a* (**a**), DO (**b**), ammonium N (**c**), nitrate N (**d**), DetN (**e**), and DetC (**f**)

increase slightly in the 300-MW experiment under current model configurations. Mechanisms for this phenomenon require further investigation in a future study.

To further quantify the impacts of tidal energy extraction on water quality, the total masses of phytoplankton, DO, and nitrate in the entire tidal bay for each experiment were calculated and compared in Fig. 9, representing key biologically important water variables for coastal ecosystems. Similar to Fig. 7, the results were first processed with a low-pass filter to remove high-frequency oscillations. As can be seen in Fig. 9, phytoplankton and DO show similar trends in which the total mass increases as more energy is extracted from the system. In contrast, nitrate shows an opposite trend with total mass decreasing as more energy is extracted. These results suggest that the extraction of tidal energy may increase phytoplankton biomass, leading to more nitrate N consumption within the water body. In addition, more oxygen may be produced in the system by increased photosynthesis. In terms of temporal variability, all three water quality variables show consistent seasonal patterns in the three experiments. For instance, the DO mass reached a minimum in late summer when water temperature is highest.

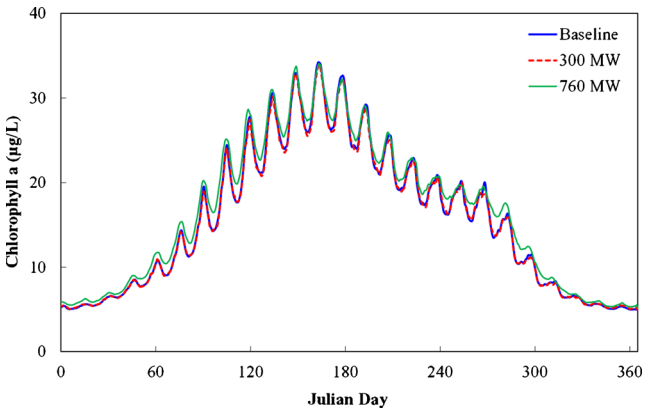

Fig. 7 Phytoplankton (chlorophyll *a*) responses to energy extraction compared with the baseline condition at the station located in the upper bay

It is well recognized that hydrodynamics may substantially modulate biological processes in estuarine and

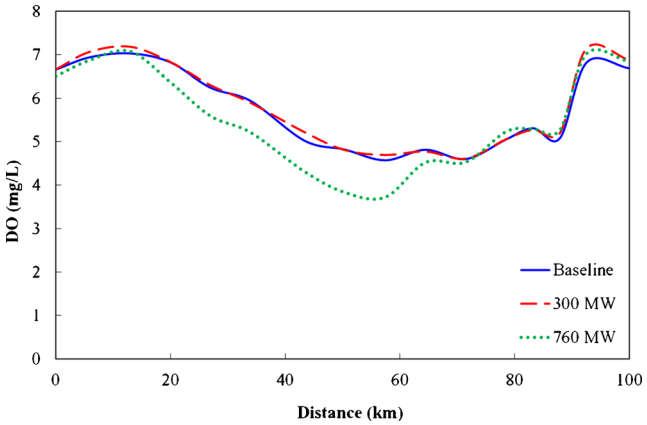

Fig. 8 Minimum daily averaged bottom DO concentrations along the longitudinal transect of the tidal bay based on the hourly model output for the entire year. Distance on the x-axis is measured from the intersection of the tidal channel and bay shown in Fig. 2

coastal ecosystems (Monbet 1992; Nixon et al. 1996). Previous studies (e.g., Yang et al. 2013) also suggest that extracting energy from a tidal system reduces the flushing rate and may indirectly affect the water quality. The flushing time was, thus, calculated for all three experiments using the freshwater displacement time method (Dyer 1973; Officer 1976; Huang 2007; Shen and Wang 2007), in which the flushing time for the entire tidal bay is defined as:

$$\mathrm{FT}(t) = \frac{V_\mathrm{f}}{Q_\mathrm{f}} = \frac{\int_\mathrm{vol} f d(V)}{Q_\mathrm{f}} \tag{20}$$

where FT is the flushing time for the entire bay (in days), V_f is the total volume of freshwater inside the tidal bay (in cubic meters) and can be calculated by integrating the freshwater volume for all the model grid cells inside the bay, Q_f is the river discharge rate (in cubic meters per second), and f is the freshwater fraction at each model grid cell and is defined as:

$$f = \frac{S_0 - S}{S_0} \tag{21}$$

where S_0 is the prescribed open boundary salinity (parts per thousand) and S is the model calculated salinity at each model grid cell.

The flushing time results are shown in Fig. 10. As one can see, flushing time increases as more power is extracted from the system. The results are also consistent with the previous study by Yang et al. (2013) and the velocity response curves shown in Fig. 5. In terms of the temporal trend, the flushing time appears to be negatively correlated with the river flow shown in Fig. 3a. This also agrees well with other studies (Huang 2007; Shen and Wang 2007) and confirms that, along with tides, river discharge plays an important role in regulating the flushing rate of a tidal system. For example, the flushing time for the baseline condition ranges from 40 days in winter and late spring to more than 120 days in summer: this variation is caused mainly by the seasonal variations of river discharge.

The longer flushing time associated with more energy extraction may act to increase phytoplankton biomass in the water body (Fig. 9a). Due to increased primary production and flushing time, hypoxia can develop in the bottom water when DO is consumed by excess organic matter. As indicated in Fig. 10, both flushing times and the differences between the three experiments reach maximum in late summer when river flow is lowest. Consequently, the negative effects of energy extraction on DO become more pronounced in late summer when water temperatures increase.

Yang and Wang (2013a) found that extracting tidal energy from the tidal channel increases vertical mixing. Because exchange between the tidal bay and the coastal ocean in the model is controlled by the channel, increased vertical mixing in the channel could subsequently affect water circulation and mass transport in the bay. Figure 11 shows the low-pass filtered time series comparisons of vertical DO differences (surface DO minus bottom DO) under different energy extraction conditions at the station located in the middle of the channel (Fig. 2). As can be seen, the vertical DO gradients decrease consistently as more energy is extracted from the channel, which agrees well with the findings by Yang and Wang (2013a). The impacts of tidal energy extraction on water quality result largely from the modulation of the hydrodynamics, in which decreased flushing rates in the bay and increased vertical mixing in the channel are the two competing processes affecting water quality responses. While increased vertical mixing may help improve bottom DO in the bay, decreased flushing rates tend to negatively affect water quality by increasing phytoplankton productivity and decreasing bottom water DO in later summer.

Summary

In this study, an unstructured-grid coastal ocean model FVCOM with built-in tidal turbine and water quality modules was applied to assess the effects of tidal energy extraction on water quality in a stratified estuarine system, consisting of a tidal bay with river inflow and a narrow channel connecting to the coastal ocean. To mimic realistic estuarine systems, the model was forced by input data constructed from observations in estuaries like Puget Sound. The effects of tidal energy extraction were examined for two energy extraction scenarios based on an efficiency curve for tidal turbines. The established baseline condition reasonably reproduced the typical water quality conditions in temperate fjords receiving relatively low nutrients from rivers. The water quality simulation results for the two energy extraction experiments suggest, in general, that

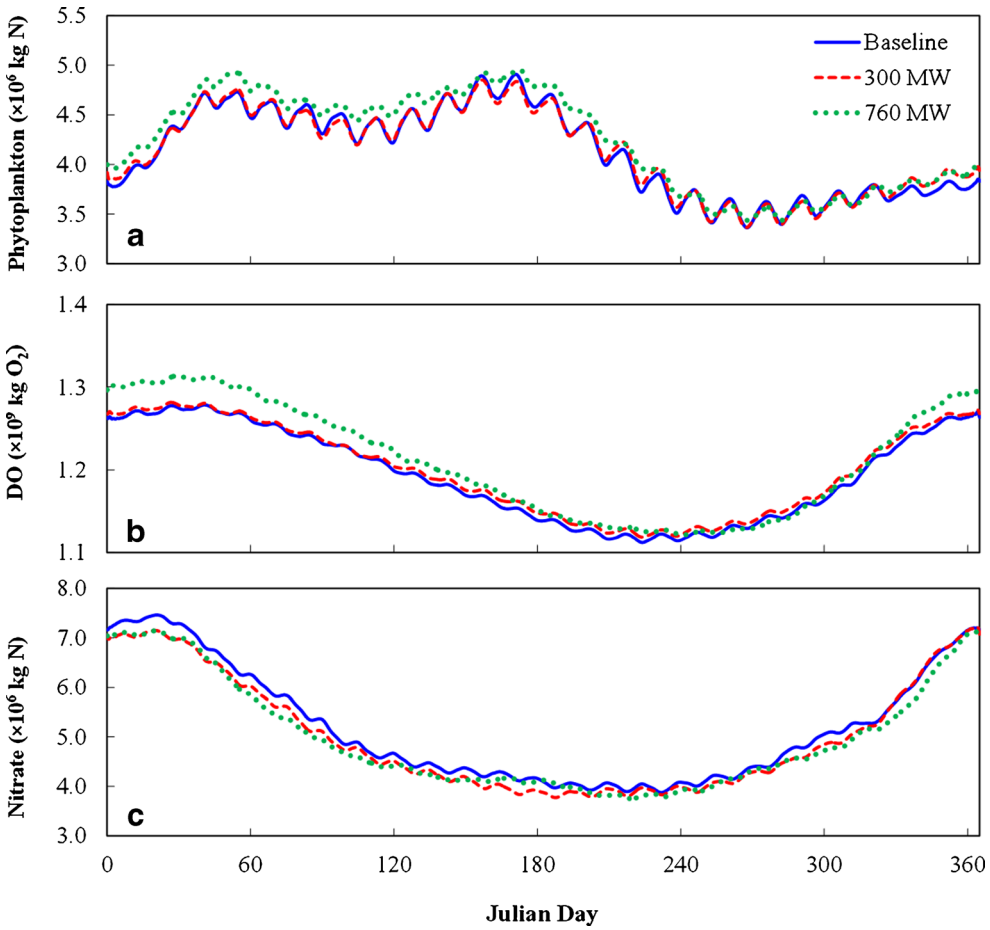

Fig. 9 Time series plot of total mass of phytoplankton (**a**), DO (**b**), and nitrate (**c**) in the bay for the three model scenarios

the effects of energy extraction on water quality are closely related to the amount of power extracted from the system. When tidal energy was extracted at a level (760 MW experiment) approaching the upper limit for the water body, unfavorable water quality conditions such as low DO could eventually develop in bottom waters. In comparison, the effects on water quality were much smaller when tidal energy was extracted at a lower level (300 MW experiment).

As the first modeling effort directly aimed at assessing the impacts of tidal energy extraction on estuarine water quality, this study provides useful information on evaluating water quality responses to tidal energy extraction using a coastal ocean model with built-in tidal turbine and water quality modules. Tidal energy extraction was found to result in

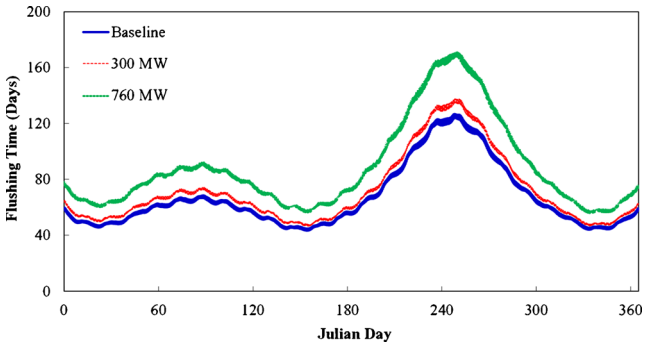

Fig. 10 Time series comparisons of flushing time of the bay calculated with the freshwater displacement time method

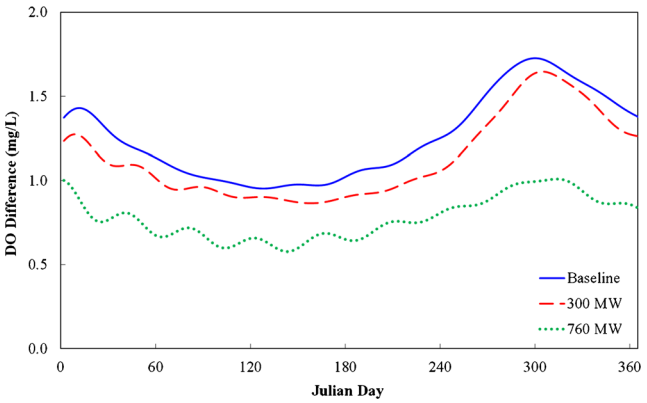

Fig. 11 Time series plot of differences of DO concentrations between surface and bottom layers for the three model scenarios at the channel station

decreased flushing rates in the bay and increased vertical mixing in the channel, with potentially greater effects on water quality from the decrease in flushing rates. This modeling effort shows interesting and important results, but also uncovers limitations. For instance, there are considerable simplifications in this study including an idealized model domain and simplified forcing data. In addition, water quality models are often associated with a high degree of uncertainty due to the complexity of biogeochemical processes. These limitations support the need for field validation data for all water quality modeling efforts, with specific emphasis on those where new perturbations such as energy extraction are under consideration. This study demonstrated that numerical models can serve as a useful tool for evaluating water quality impacts associated with tidal energy extraction. Additionally, more careful efforts are warranted to address system-specific environmental issues in complex real estuarine environments, including the implications of primary productivity and associated water quality conditions with higher-level organisms in the marine food web.

Acknowledgments This study was funded by the Wind and Water Power Program under the Office of Energy Efficiency and Renewable Energy, US Department of Energy. The authors would like to thank the reviewers for their help in improving the quality of the manuscript. Dr. Changsheng Chen at University of Massachusetts Dartmouth is also acknowledged for providing the authors the FVCOM source code.

References

Atwater, J., and G. Lawrence. 2010. Power potential of a split tidal channel. *Renewable Energy* 35: 329–332.

Bianucci, L., K. Denman, and D. Ianson. 2011. Low oxygen and high organic carbon on the Vancouver Island Shelf. *Journal of Geophysical Research* 116, C07011.

Blanchfield, J., C. Garrett, P. Wild, and A. Rowe. 2008. The extractable power from a channel linking a bay to the open ocean. *Proceedings of the Institution of Mechanical Engineers, Part A: Journal of Power and Energy* 222: 289–297.

Bowie, G.L., W.B. Mills, D.B. Porcella, C.L. Campbell, J.R. Pagenkopt, G.L. Rupp, K.M. Johnson, P.W.H. Chan, and S.A. Gherini. 1985. *Rates, constants and kinetics formulations in surface water quality modeling*, 2nd ed. Athens: US Environmental Protection Agency. EPA 600/3-85/040.

Bryden, I., and S. Couch. 2007. How much energy can be extracted from moving water with a free surface: A question of importance in the field of tidal current energy? *Renewable Energy* 32: 1961–1966.

Cerco, C., and T. Cole. 1993. Three-dimensional eutrophication model of Chesapeake Bay. *ASCE Journal of Environmental Engineering* 119: 1006–1025.

Cerco, C. and T. Cole. 1994. Three-dimensional eutrophication model of Chesapeake Bay: Volume 1, main report. Technical Report EL-94-4, US Army Engineer Waterways Experiment Station, Vicksburg.

Cerco, C. and M. Noel. 2004. The 2002 Chesapeake Bay eutrophication model. Report No. EPA 903-R-04-004.

Chen, C., H. Liu, and R.C. Beardsley. 2003. An unstructured, finite-volume, three-dimensional, primitive equation ocean model: Application to coastal ocean and estuaries. *Journal of Atmospheric and Oceanic Technology* 20: 159–186.

Chen, C., R. Beardsley, and G. Cowles. 2006. An unstructured grid, finite-volume coastal ocean model: FVCOM user manual. School for Marine Science and Technology, University of Massachusetts Dartmouth, 315 pp.

Chen, C., H. Huang, R. Beardsley, H. Liu, Q. Xu, and G. Cowles. 2007. A finite volume numerical approach for coastal ocean circulation studies: Comparisons with finite difference models. *Journal of Geophysical Research* 112, C03018. doi:10.0129/2006JC003485.

Chen, C., G. Gao, J. Qi, A. Proshutinsky, R. Beardsley, Z. Kowalik, H. Lin, and G. Cowles. 2009. A new high-resolution unstructured-grid finite-volume Arctic Ocean model (AO-FVCOM): an application for tidal studies. *Journal of Geophysical Research*. doi:10.1029/2008jc004941.

Chen, C., Z. Lai, R. Beardsley, Q. Xu, H. Lin, and N. Viet. 2012. Current separation and upwelling over the southeast shelf of Vietnam in the South China Sea. *Journal of Geophysical Research Oceans* 117. doi:10.1029/2011JC007150.

Cole, T. and S. Wells. 2009. CE-QUAL-W2: A two-dimensional, laterally averaged, hydrodynamic and water quality model, version 3.6 user manual. Instruction Report EL-08-1, US Army Corps of Engineers, Washington, DC.

Defne, Z., K.A. Haas, and H.M. Fritz. 2011. Numerical modeling of tidal currents and the effects of power extraction on estuarine hydrodynamics along the Georgia coast, USA. *Renewable Energy* 36: 3461–3471.

Draper, S., G. Houlsby, M. Oldfield, and A. Borthwick. 2009. Modeling tidal energy extraction in a depth-averaged coastal plain. Proceedings of the 8th European Wave and Tidal Energy Conference, Uppsala, Sweden, p. 1045–1052.

Dyer, K. 1973. *Estuaries: A physical introduction*. New York: Wiley.

Fennel, K., J. Wilkin, J. Levin, J. Moisan, J. O'Reilly, and D. Haidvogel. 2006. Nitrogen cycling in the Middle Atlantic Bight: Results from a three-dimensional model and implications for the North Atlantic nitrogen budget. *Global Biogeochemical Cycles* 20, GB3007.

Garrett, C., and P. Cummins. 2005. The power potential of tidal currents in channels. *Proceedings of Royal Society A* 461: 2563–2572.

Garrett, C., and P. Cummins. 2008. Limits to tidal current power. *Renewable Energy* 33: 2485–2490.

Gorlov, A. 2001. *Tidal energy. In: Encyclopedia of ocean sciences*, 2955–2960. Oxford: Academic.

Grabbe, M., E. Lalander, S. Lundin, and M. Leijon. 2009. A review of the tidal current energy resource in Norway. *Renewable and Sustainable Energy Reviews* 13: 1898–1909.

Gruber, N., H. Frenzel, S. Doney, P. Marchesiello, J. McWilliams, J. Moisan, J. Oram, G.-K. Plattner, and K. Stolzenbach. 2006. Eddy-resolving simulation of plankton ecosystem dynamics in the California Current System. *Deep-Sea Research I* 53: 1483–1516.

Hasegawa, D., J. Sheng, D. Greenberg, and K. Thompson. 2011. Far-field effects of tidal energy extraction in the Minas Passage on tidal circulation in the Bay of Fundy and Gulf of Maine using a nested-grid coastal circulation model. *Ocean Dynamics* 61: 1845–1868.

Hu, S., C. Chen, R. Ji, D.W. Townsend, R. Tian, R. Beardsley, and C. Davis. 2011. Effects of surface forcing on interannual variability of the fall phytoplankton bloom in the Gulf of Maine revealed using a process-oriented model. *Marine Ecological Progress Series* 427: 29–49.

Huang, W. 2007. Hydrodynamic modeling of flushing time in a small estuary of North Bay, Florida, USA. *Estuarine, Coastal and Shelf Science* 74: 722–731.

Ji, R., C. Davis, C. Chen, and R. Beardsley. 2008. Influence of local and external processes on the annual nitrogen cycle and primary productivity on Georges Bank: A 3-D biological–physical modeling study. *Journal of Marine System* 73: 31–47.

Kadiri, M., R. Ahmadian, B. Bockelmann-Evans, W. Rauen, and R. Falconer. 2012. A review of the potential water quality impacts of tidal renewable energy systems. *Renewable and Sustainable Energy Reviews* 16: 329–341.

Karsten, R., J. McMillan, M. Lickley, and R. Haynes. 2008. Assessment of tidal current energy in the Minas Passage, Bay of Fundy. *Proceedings of the Institution of Mechanical Engineers, Part A: Journal of Power and Energy* 222: 493–507.

Monbet, Y. 1992. Control of phytoplankton biomass in estuaries: A comparative analysis of microtidal and macrotidal estuaries. *Estuaries* 15: 563–571.

Newton, J., C. Bassin, A. Devol, M. Kawase, W. Ruef, M. Warner, D. Hannafious, and R. Rose. 2007. Hypoxia in Hood Canal: An overview of status and contributing factors. In: Proceedings of 2007 George Basin Puget Sound Research Conference, Vancouver, British Columbia, 26–29 March 2007.

Nixon, S.W., J.W. Ammerman, L.P. Atkinson, V.M. Berounsky, G. Billen, W.C. Biocourt, W. Boynton, T.M. Church, D.M. Ditoro, R. Elmgren, J.H. Garber, A.E. Giblin, R.A. Jahnke, N.J.P. Owens, M.E.Q. Pilson, and S.P. Seitzinger. 1996. The fate of nitrogen and phosphorus at the land–sea margin of the North Atlantic Ocean. *Biogeochemistry* 35: 141–180.

Officer, C. 1976. *Physical oceanography of estuaries (and associated coastal waters)*. New York: Wiley.

Officer, C., R. Biggs, J. Taft, L. Cronin, M. Tyler, and W. Boynton. 1984. Chesapeake Bay anoxia: Origin, development and significance. *Science* 223: 22–27.

O'Rourke, F., F. Boyle, and A. Reynolds. 2010. Tidal current energy resource assessment in Ireland: Current status and future update. *Renewable and Sustainable Energy Reviews* 14: 3206–3212.

Park, K., A. Kuo, J. Shen, and J. Hamrick. 1995. A three-dimensional hydrodynamic-eutrophication model HEM-3D: Description of water quality and sediment process submodels. SRAMSOE No. 327, Virginia Institute of Marine Science, Gloucester Point, VA.

Park, K., H.-S. Jung, H.-S. Kim, and S.-M. Ahn. 2005. Three-dimensional hydrodynamic–eutrophication model (HEM-3D): Application to Kwang-Yang Bay, Korea. *Marine Environmental Research* 60: 171–193.

Parker, D. 1993. Environmental implications of tidal power generation. *IEE Proceedings-A* 140: 71–75.

Shapiro, G. 2010. Effect of tidal stream power generation on the region-wide circulation in a shallow sea. *Ocean Science Discussions* 7: 1785–1810.

Shen, J., and H. Wang. 2007. Determining the age of water and long-term transport timescale of the Chesapeake Bay. *Estuarine, Coastal and Shelf Science* 74: 750–763.

Sutherland, G., M. Foreman, and C. Garrett. 2007. Tidal current energy assessment for Johnstone Strait, Vancouver Island. *Proceedings of the Institution of Mechanical Engineers, Part A: Journal of Power and Energy* 221: 147–157.

Walkington, I., and R. Burrows. 2009. Modeling tidal stream power potential. *Applied Ocean Research* 31: 239–245.

Wang, S., Y. Peng, D. Li, and Y. Jiao. 2011. An overview of ocean renewable energy in China. *Renewable and Sustainable Energy Reviews* 15: 91–111.

Weisberg, R., and L. Zheng. 2006. Hurricane storm surge simulation for Tampa Bay. *Estuaries and Coasts* 29(6A): 899–913.

Yang, Z., T. Khangaonkar, and T. Wang. 2011. Use of advanced meteorological model output for coastal ocean modeling in Puget Sound. *International Journal of Climate and Ocean Systems* 2: 101–117.

Yang, Z., T. Wang, T. Khangaonkar, and S. Breithaupt. 2012. Integrated modeling of flood flows and tidal hydrodynamics over a coastal floodplain. *Environmental Fluid Mechanics* 12: 63–80.

Yang, Z., and T. Wang. 2013a. Modeling the effects of tidal energy extraction on estuarine hydrodynamics in a stratified estuary. *Estuaries and Coasts*. doi:10.1007/s12237-013-9684-2.

Yang, Z., and T. Wang. 2013b. Tidal residual eddies and their effect on water exchange in Puget Sound. *Ocean Dynamics* 63: 995–1009. doi:10.1007/s10236-013-0635-z.

Yang, Z., T. Wang, and A. Copping. 2013. Modeling tidal stream energy extraction and its effects on transport processes in a tidal channel and bay system using a three-dimensional coastal ocean model. *Renewable Energy* 50: 605–613.